

## Discovery and Rossiter-McLaughlin Effect of Exoplanet Kepler-8b<sup>0</sup>

Jon M. Jenkins<sup>2</sup>, William J. Borucki<sup>1</sup>, David G. Koch<sup>1</sup>, Geoffrey W. Marcy<sup>3</sup>,  
William D. Cochran<sup>8</sup>, Gibor Basri,<sup>3</sup> Natalie M. Batalha<sup>4</sup>, Lars A. Buchhave<sup>5,6</sup>, Tim M. Brown<sup>7</sup>,  
Douglas A. Caldwell<sup>2</sup>, Edward W. Dunham<sup>9</sup>, Michael Endl<sup>8</sup>, Debra A. Fischer<sup>10</sup>,  
Thomas N. Gautier III<sup>11</sup>, John C. Geary<sup>5</sup>, Ronald L. Gilliland<sup>12</sup>, Steve B. Howell<sup>13</sup>,  
Howard Isaacson<sup>3</sup>, John Asher Johnson<sup>14</sup>, David W. Latham<sup>5</sup>, Jack J. Lissauer<sup>1</sup>,  
David G. Monet<sup>15</sup>, Jason F. Rowe<sup>1,16</sup>, Dimitar D. Sasselov<sup>5</sup>, William F. Welsh<sup>17</sup>,  
Andrew W. Howard<sup>3</sup>, Phillip MacQueen<sup>8</sup>, Hema Chandrasekaran<sup>2</sup>, Joseph D. Twicken<sup>2</sup>,  
Stephen T. Bryson<sup>1</sup>, Elisa V. Quintana<sup>2</sup>, Bruce D. Clarke<sup>2</sup>, Jie Li<sup>2</sup>, Christopher Allen<sup>18</sup>,  
Peter Tenenbaum<sup>2</sup>, Hayley Wu<sup>2</sup>, Soren Meibom<sup>5</sup>, Todd C. Klaus<sup>18</sup>, Christopher K. Middelour<sup>18</sup>,  
Miles T. Cote<sup>1</sup>, Sean McCauliff<sup>18</sup>, Forrest R. Girouard<sup>18</sup>, Jay P. Gunter<sup>18</sup>, Bill Wohler<sup>18</sup>,  
Jennifer R. Hall<sup>18</sup>, Khadeejah Ibrahim<sup>18</sup>, AKM Kamal Uddin<sup>18</sup>, Michael S. Wu<sup>19</sup>,  
Paresh A. Bhavsar<sup>1</sup>, Jeffrey Van Cleve<sup>2</sup>, David L. Pletcher<sup>1</sup>, Jessie A. Dotson<sup>1</sup>, Michael R. Haas<sup>1</sup>

---

<sup>0</sup>Based in part on observations obtained at the W. M. Keck Observatory, which is operated as a scientific partnership among the California Institute of Technology, the University of California, and the National Aeronautics and Space Administration. The Observatory was made possible by the generous financial support of the W.M. Keck Foundation.

## ABSTRACT

We report the discovery and the Rossiter-McLaughlin effect of Kepler-8b, a transiting planet identified by the NASA *Kepler Mission*. *Kepler* photometry and Keck-HIRES radial velocities yield the radius and mass of the planet around this F8IV subgiant host star. The planet has a radius  $R_p = 1.419 R_J$  and a mass,  $M_p = 0.60 M_J$ , yielding a density of  $0.26 \text{ g cm}^{-3}$ , among the lowest density planets known. The orbital period is  $P = 3.523$  days and orbital semimajor axis is  $0.0483^{+0.0006}_{-0.0012}$  AU. The star has a large rotational  $v \sin i$  of  $10.5 \pm 0.7 \text{ km s}^{-1}$  and is relatively faint ( $V \approx 13.89$  mag), both properties deleterious to precise Doppler measurements. The velocities are indeed noisy, with scatter of  $30 \text{ m s}^{-1}$ , but exhibit a period and phase consistent with the planet implied by the photometry. We securely detect the Rossiter-McLaughlin effect, confirming the planet’s existence and establishing its orbit as prograde. We measure an inclination between the projected planetary orbital axis and the projected stellar rotation axis of  $\lambda = -26.9 \pm 4.6^\circ$ , indicating a moderate inclination of the planetary orbit. Rossiter-McLaughlin measurements of a large sample of transiting planets from *Kepler* will provide a statistically robust measure of the true distribution of spin-orbit

---

<sup>1</sup>NASA Ames Research Center, Moffett Field, CA 94035

<sup>2</sup>SETI Institute/NASA Ames Research Center, Moffett Field, CA 94035

<sup>3</sup>University of California, Berkeley, Berkeley, CA 94720

<sup>4</sup>San Jose State University, San Jose, CA 95192

<sup>5</sup>Harvard-Smithsonian Center for Astrophysics, 60 Garden Street, Cambridge, MA 02138

<sup>6</sup>Niels Bohr Institute, Copenhagen University, DK-2100 Copenhagen, Denmark

<sup>7</sup>Las Cumbres Observatory Global Telescope, Goleta, CA 93117

<sup>8</sup>University of Texas, Austin, TX 78712

<sup>9</sup>Lowell Observatory, Flagstaff, AZ 86001

<sup>10</sup>Radcliffe Institute, Cambridge, MA & Yale University, New Haven, CT

<sup>11</sup>Jet Propulsion Laboratory/California Institute of Technology, Pasadena, CA 91109

<sup>12</sup>Space Telescope Science Institute, Baltimore, MD 21218

<sup>13</sup>National Optical Astronomy Observatory, Tucson, AZ 85719

<sup>14</sup>California Institute of Technology, Pasadena, CA 91109

<sup>15</sup>US Naval Observatory, Flagstaff Station, Flagstaff, AZ 86001

<sup>16</sup>NASA Postdoctoral Fellow Program

<sup>17</sup>San Diego State University, San Diego, CA

<sup>18</sup>Orbital Sciences Corporation/NASA Ames Research Center, M/S 244-30, Moffett Field, CA 94035, USA

<sup>19</sup>Bastion Technologies/NASA Ames Research Center, M/S 244-30, Moffett Field, CA 94035, USA

orientations for hot jupiters in general.

*Subject headings:* planetary systems — stars: fundamental parameters — stars: individual (Kepler-8, KIC 6922244, 2MASS 18450914+4227038)

## 1. Introduction

To date, 90 “hot jupiters”—gas giant planets with periods  $\leq 10$  days—have been detected around Sun-like stars (Torres et al. 2008). The front-running formation scenario supposes that these planets did not form where they reside today, close the host star, because the inner regions of protoplanetary disks have inadequate surface densities and high temperatures (Lin et al. 1996). Instead hot jupiters are presumed to form several astronomical units (AU) from their host stars followed by subsequent migration inward to their current locations. One likely migration scenario involves tidal interactions between the planet and a remaining gaseous disk (Lin et al. 1996; Moorhead & Adams 2008), causing the planet to spiral inward while maintaining its nearly circular orbit that is co-planar with the disk. Alternatively, migration may occur by N-body gravitational interactions, such as planet–planet scattering (Rasio & Ford 1996; Chatterjee et al. 2008), dynamical relaxation (Papaloizou & Terquem 2001; Adams & Laughlin 2003), and Kozai interactions with a distant object, and damped later by tidal friction (Holman et al. 1997; Fabrycky & Tremaine 2007; Wu et al. 2007; Nagasawa et al. 2008). Thus, measurements of both the orbital eccentricities and the orbital inclinations relative to the star’s equator offer diagnostics of the original migration process.

We assume that planets form in protoplanetary disks with the stellar spin and planetary orbital axes aligned. If so, the nearly adiabatic tidal interactions between planets and disks would maintain the alignment (Ward & Hahn 1994). In contrast, few-body gravitational interactions would typically cause misalignments. Few-body models by Adams & Laughlin (2003) predict a final inclination distribution for dynamically relaxed planetary systems that peaks near  $20^\circ$  and which extends to inclinations as high as  $85^\circ$ . Kozai interactions between a planet and an outer body (star or planet) result in a wide distribution of final orbital inclinations for the inner planet, including retrograde orbits (Fabrycky & Tremaine 2007; Wu et al. 2007; Nagasawa et al. 2008).

The Rossiter-McLaughlin (R-M) effect offers a way to assess quantitatively the spin-orbit alignment of a planetary system by measuring the Doppler effect of the star’s light during a planetary transit. As the planet blocks receding portion of a rotating star’s surface, the spectrum from the unobscured surface has a net Doppler shift toward shorter wavelengths, and vice versa for blocking the approaching portion of the star. The R-M effect has been measured in 18 stars to date (Queloz et al. 2000; Winn et al. 2005, 2006, 2007; Wolf et al. 2007; Narita et al. 2007, 2008; Bouchy et al. 2008; Cochran et al. 2008; Loeillet et al. 2008; Winn et al. 2008; Johnson et al. 2009; Pont et al. 2009; Moutou et al. 2009; Pont et al. 2009; Winn et al. 2009; Narita et al. 2009a,b; Simpson et al. 2010; Anderson et al. 2009; Gillon 2010; Pont et al. 2009; Amaury, A. et al. 2010).

About 2/3 of the 18 planetary systems measured by the R-M effect have an orbital plane well aligned with the star’s equatorial plane, as projected onto the sky, giving  $\lambda$  near  $0^\circ$ . This alignment is as expected from simple migration theory due to gentle loss of orbital energy to the gas in the protoplanetary disk (Lin et al. 1996). However, six exoplanetary systems show a significant spin-orbit misalignment, namely HD 80606 (Winn et al. 2009; Moutou et al. 2009; Pont et al. 2009; Gillon 2010), WASP-14b (Johnson et al. 2009; Joshi et al. 2009), XO-3b (Hébrard et al. 2009; Winn et al. 2009), HAT-P-7b (Winn et al. 2009; Narita et al. 2009a), CoRoT-1 (Pont et al. 2009) Wasp-17b (Anderson et al. 2009).

The variety of alignments support the bimodal distribution found by Fabrycky & Winn (2009). Interestingly, all four misaligned systems contain quite massive planets, above  $1 M_J$ . This correlation may be related to the association of massive planets with higher orbital eccentricity (Wright et al. 2009), as both eccentricity and inclination may arise from perturbations of planets from their original circular orbits. But there are two massive planets on eccentric orbits for which  $\lambda$  appears to be consistent with zero, namely HD 17156b (Cochran et al. 2008; Barbieri et al. 2009; Narita et al. 2009b), and HATp-2b (Winn et al. 2007; Loeillet et al. 2008). There is currently no dominant and secure explanation for the misaligned or eccentric hot jupiters.

Here, we present the first detection of the Rossiter-McLaughlin effect from a planet detected by the *Kepler Mission*. As this mission is expected to detect dozens of transiting hot jupiters, *Kepler* offers an opportunity to provide a statistically robust measure of the distribution of spin-orbit angles, and to correlate that angle with other physical properties of the systems.

## 2. *Kepler* Photometry

Nearly continuous photometry in a 100 square degrees field near Cygnus and Lyra was carried out during 42 days by the *Kepler* spaceborne telescope, as described previously (Borucki et al. 2010; Borucki et al. 2010; Koch et al. 2010; Jenkins et al. 2010; Batalha et al. 2010; Gautier et al. 2010). The star Kepler-8 (= KIC 6922244,  $\alpha = 18^{\text{h}}45^{\text{m}}09^{\text{s}}.15$ ,  $\delta = +42^\circ27'03''.9$ , J2000, KIC  $r = 13.511$  mag) exhibits a repeated dimming of  $9.82 \pm 0.22$ millimag, obvious against uncertainties in each 30 minute integration of 0.1 millimag. The light curve for Kepler-8 is plotted in Figure 1. The numerical data are available electronically in the online edition of the journal. A modest amount of detrending has been applied (Koch et al. 2010; Rowe et al. 2010) to the time series.

We detect no systematic difference between alternating transit events at  $50 \mu\text{mag}$  levels, ruling out nearly equal components of an eclipsing binary star, (see Fig. 1). We also see no evidence of dimming at the expected times of a secondary eclipse, which would be visible for most eclipsing binary systems of unequal surface brightness. The photocenter shows no displacement astrometrically above millipixel levels (0.5 mas) during times in and out of transit as would be seen if there were a background eclipsing binary masquerading as a transiting planet. Thus the photometric and astrometric non-detections of an eclipsing binary support the planet interpretation for the re-

peated transit signatures. Moreover, the shape of the photometric transit is adequately fit with a planet-transit model further supporting the planet interpretation.

We fit the light curves by solving for  $a/R_{\text{Star}}$ , the density of the star, and the ratio of planet to stellar radius. We follow the method for estimating stellar radii and other stellar parameters described by Sozzetti et al. (2007), Bakos et al. (2007), Winn et al. (2007) and Charbonneau et al. (2007). This method extracts physical properties directly from the light curve, geometry, and Newtonian physics, and it uses the greater orthogonality of parameters to yield more robust fits to observables (Torres et al. 2008). We fit explicitly for  $a/R_{\star}$ ,  $b$ , and  $r/R_{\star}$  using a procedure developed by one of us (J.Rowe) and described by Koch et al. (2010); Borucki et al. (2010).

We begin with an LTE spectroscopic analysis (Valenti & Piskunov 1996; Valenti & Fischer 2005) of a high resolution template spectrum from Keck-HIRES of Kepler-8 to derive an effective temperature,  $T_{\text{eff}} = 6213 \pm 150$  K, surface gravity,  $\log g = 4.28 \pm 0.10$ (cgs), metallicity, and the associated error distribution for each of them. The multitude of Yale-Yonsei stellar evolution models (Demarque et al. 2004) are constrained by both those LTE measurements and by the stellar density that stems directly from the orbital period, the fractional dimming during transit, and measures of transit durations (Sozzetti et al. 2007; Brown et al. 2010). By Monte Carlo analysis, those photometric and spectroscopic constraints and their uncertainties establish the probability density contours among the evolutionary tracks where the star may reside. We iterate the self-consistent fitting of light curves, radial velocities, and evolutionary models until a domain of stellar mass, radius, and age is identified. That domain encompasses a range of evolutionary states that satisfy all of the constraints within their error distributions. The resulting mass and radius of Kepler-8 are given in Table 1, along with other associated stellar properties such as luminosity and age.

### 3. A Background Eclipsing Binary: Follow-up Imaging

We carried out extensive tests of the possibility that the apparent photometric transit was actually caused by a background eclipsing binary star within the photometric aperture of radius  $\sim 8''$ . We obtained images with 0.8 arcsec seeing with the Keck telescope HIRES guider camera and the bg38 filter to search for stellar companions that might be eclipsing. This filter combined with the CCD detector have a response similar to the V plus R bands, in turn similar to the bandpass of the *Kepler* photometer. This Keck image is shown in 2. There is one star having 0.0075 the flux of the main star (V and R band) that resides  $3.8''$  northwest of Kepler-8. This background star resides within the *Kepler* aperture and could conceivably be an eclipsing binary that is masquerading as a transiting planet.

But this faint neighboring star cannot be the source of the photometric transit signature for two reasons. If the background star were the cause of the observed 1% dimming, the photocenter centroid shifts would be 3-20 millipixel on the *Kepler* CCD. Instead, astrometric measurements in and out of transit (Jenkins et al. 2010) show shifts of no more than 0.1 millipixel in and out of

transit. Figure 3 shows both the flux and astrometric photocenter (centroid) of the *Kepler* images during quarter 1 month of data. We applied a high-pass filter to remove non-transit signatures on timescales longer than 2 days. At times of transits there are no displacements in either the row or column direction at a level above a millipixel. This indicates that any background eclipsing binary would need to be well within  $\sim 0.1$  pixels or  $0.4''$  of the target star in order to explain the photometric transit signals.

To hunt further for background eclipsing binaries we plotted flux versus the photocenter centroids in both the row and column directions, as shown in Figure 4. These so-called “rain plots” would reveal an eclipsing binary as a “breeze” in the centroids to the left or right as the flux drops. No such breeze is detected at a level near 0.1 millipixel, ruling out all but eclipsing binaries located within a few tenths of an arcsec of Kepler-8. Finally, we looked directly at the *Kepler* images taken both during and out of transit to detect motion of the centroid of light, as shown in Figure 5. We formed the difference of the images in and out of transit to detect astrometric displacements associated with the flux dimming, as would occur if a neighboring eclipsing binary were the cause. Those difference images show no shift of the photocenter. We conclude that the transit photometry with its 1% dimming cannot be explained by any eclipsing binary companions beyond 1 arcsecond of Kepler-8.

Furthermore, the flux ratio of the two stars is only 0.0075, making it impossible for the background star to cause the 1% photometric dimming. Even if that background star were to vanish, the total flux would decline by less than the observed 1%. We conclude that the 1% photometric dimming is not caused by an eclipsing binary star within the *Kepler* photometric aperture, from 1 - 10 arcsec of the target star.

To hunt for additional stars in the field within an arcsec of Kepler-8 we used both speckle imaging and adaptive optics imaging. Kepler-8 was observed at the Palomar Hale 200-inch telescope on 09 Sep 2009 UT with Palomar near-infrared adaptive optics system [PHARO] (Hayward et al. 2001). The PHARO instrument was utilized in the J-band filter with the 25 mas per pixel ( $25''$ FOV) mode. The source was observed with a 5-point dither and an integration time of 2.8 seconds per frame. The dither pattern was repeated 7 times for a total on-source integration time of 98 seconds. The average uncorrected seeing during the observations at J-band was  $0.65''$ , and the average AO corrected images produced point spread functions that were  $0.09''$ FWHM. There are two faint sources within  $4''$  of Kepler-8; these objects are 7 and 8.4 magnitudes fainter than the primary target and are too faint to produce the *Kepler*-observed transit and centroid shift. The AO imaging detected no sources at J-band down to within  $0.1'' - 0.2''$  of the primary target that are within  $\Delta m \approx 6 - 7$  mag at J.

Speckle observations of Kepler-8 were made on 1 October 2009 (UT) at the WIYN observatory located on Kitt Peak. The observations were made using the WIYN speckle camera during a night of very good seeing ( $0.62''$ ) and under clear conditions. We used a narrow bandpass 40 nm wide centered at 692 nm. The Kepler speckle program obtains observations of both double and single

standard stars throughout the night. We use a robust background estimator on the reconstructed images to set a limit for the level of companion star we should detect if present. The speckle observations show that Kepler-8 has no companion star between 0.05 and 2.0 arcsec within a delta magnitude of  $<4.2$  mags. These AO and speckle observations effectively rule out the possibility of an eclipsing binary star to within as close as 0.1 arcsec from Kepler-8.

### 3.1. Covariance of Inclination, Limb Darkening, and Stellar Parameters

As Kepler-8 has a large impact parameter, the solution is quite sensitive to errors in limb-darkening. The derived impact parameter and inclination angle are directly related to the assumed limb-darkening law, poorly known for the wide *Kepler* bandpass. We adopted an adhoc approach to estimate the limb-darkening parameters (Rowe et al. 2010) as follows. We noted that fits to the observed Rossiter-McLaughlin effect (see section 6), coupled with the measured  $v \sin i = 10.5 \pm 0.7$   $\text{km s}^{-1}$  offered a constraint on the inclination angle and the impact parameter, and hence on the inferred stellar radius, for a given limb-darkening law. To solve the general case for eccentric orbits see Pal et al. (2010).

For the cases of Kepler-4 and Kepler-5 (Borucki et al. 2010; Koch et al. 2010), we discovered that a model using tabular values (Prsa & Zwitter 2006) for limb darkening over-predicted the amount of curvature in the variation of flux as a function of time during transit. We therefore modified the limb-darkening parameters by fitting the three known exoplanets, TRES-2, HAT-P-7, and HAT-P-11, and using published values for their stellar and planetary parameters. We linearly interpolated over the values of effective temperature to derive a superior measure of the true limb-darkening law for the *Kepler* bandpass. The photometry from new transiting planets found by *Kepler*, along with IR photometry that is less sensitive to limb darkening, will allow us to refine the limb-darkening law for the *Kepler* bandpass in the coming months. The resulting fits to the photometric transits of Kepler-4, 5, 6, 7, and 8 were all improved with our new limb-darkening treatment (Rowe et al. 2010).

For Kepler-8, the resulting impact parameter and inclination were  $b=0.724 \pm 0.020$  and  $i = 84.07 \pm 0.33$  both about 10% smaller than we had obtained by using the first-guess limb-darkening law. The transit duration in turn dictates the best-fit stellar radius, and after iterating with the Yale-Yonsei models, the resulting stellar radius is  $R = 1.486_{-0.062}^{+0.053} R_{\odot}$ . The stellar mass has a value within a narrow range,  $M = 1.213_{-0.063}^{+0.067} M_{\odot}$ , again derived from iteration between the fit to the light curve and to the Yale-Yonsei models. Additional information on stellar mass comes from the projected rapid rotation of the star,  $v \sin i = 10.5 \pm 0.7$   $\text{km s}^{-1}$ . This  $v \sin i$  is faster than typical rotation for stars at the lower end of the mass range quoted above, especially as some evolution and associated increase in moment of inertia has occurred. Thus we marginally favor the upper half of the quoted mass range, i.e.  $M > 1.213 M_{\odot}$ . The stellar gravity is  $\log g = 4.174 \pm 0.026$  (cgs), and the approximate age is  $3.84 \pm 1.5$  Gyr, both indicating a star nearing the end of its main sequence lifetime.

#### 4. Radial Velocities

We took high resolution spectra of Kepler-8 using HIRES on the Keck I 10-m telescope (Vogt et al. 1994). We set up the HIRES spectrometer in the same manner that has been used consistently for 10 years with the California planet search (Marcy et al. 2008). We employed the red cross-disperser and used the I<sub>2</sub> absorption cell to measure the instrumental profile and the wavelength scale. The slit width was set at 0".87 by the "B5 decker", giving a resolving power of about 60,000 at 5500Å. Between 2009 June 1 and 2009 October 31 we gathered 15 spectra of Kepler-8 out of transit (See Figure 6). Typical exposure times were between 10 - 45 min, yielding signal-to-noise of 20 - 40 pixel<sup>-1</sup>. These are quite low S/N ratios with which to attempt precise Doppler measurements. We tested the Doppler precision from such low SNR spectra on standard stars, notably HD 182488 and HD 9407, and found that the expected errors are ~5 m s<sup>-1</sup>, as expected from Poisson statistics of the photons, with no systematic errors above 1 m s<sup>-1</sup>, as usual for the iodine technique. On 2009 October 29 (UT) we obtained nine spectra of Kepler-8 during transit (the last taken during egress). The observations were taken between airmass 1.9 and 3.8, while the star was setting, the last exposure occurring at hour angle 5 hr 35 min with extreme atmospheric refraction and dispersion. Again, tests with standard stars observed at such high airmass show no systematic errors in the Doppler measurements above 1 m s<sup>-1</sup>.

We carried out careful reduction of the raw images, including cosmic ray elimination and optimal extraction of the spectra, to minimize the background moonlight. We performed the Doppler analysis with the algorithm of Johnson et al. (2009). We estimated the measurement error in the Doppler shift derived from a given spectrum based on the weighted standard deviation of the mean among the solutions for individual 2 Å spectral segments. The typical internal measurement error was 7-10 m s<sup>-1</sup>. The resulting velocities are given in Table 2 and plotted in Figure 6.

The actual uncertainties in the velocities are certainly closer to 20-25 m s<sup>-1</sup> for several reasons. The spectra have such low photon levels, ~200 photons per pixel in the raw CCD images, that cosmic rays and background sky are significant noise sources. The latter was especially problematic as we used an entrance slit with dimensions 0.87 x 3.5 arcsec, not long enough to separate the wings of the star's point spread function from the background sky. Nearly all HIRES spectra were taken with the moon gibbous or full, and about half of the nights had moderate cirrus that scatters moonlight into the slit. A few observations made with a 14 arcsec slit revealed that 1-3% of the light came from the moonlit sky in typical observations. Simulations with stellar spectra contaminated by moonlit sky suggested that errors of ~10 m s<sup>-1</sup> would accrue, no doubt systematic as well. Errors in the velocities are large because of relatively rapid rotation,  $v \sin i = 10.5 \pm 0.7$ , broadening the absorption lines by 5x that of the slowest rotating stars. Doppler errors increase linearly with line widths. Thus, while the S/N=40 might be expected to yield velocities of ~5 m s<sup>-1</sup>, the high  $v \sin i$  increases that error to ~25 m s<sup>-1</sup>. Indeed, the best orbital fit to the velocities, shown in Figure 6, exhibit discrepancies of 20-30 m s<sup>-1</sup>. We estimate that the true errors in velocities are thus ~25 m s<sup>-1</sup>. We have accounted for these errors by adding a "jitter" of 25 m s<sup>-1</sup> to the internal velocity errors. Those augmented uncertainties are reflected in Table 2.

We carried out a Levenberg-Marquardt least-squares fit of a Keplerian, single-planet model to the observed velocities. In all models the orbital period and the time of mid-transit was constrained to be that found in the photometric fit. We first assumed a circular orbit leaving only two free parameters in our fit, namely the velocity amplitude and the gamma velocity of the system. The best-fit model is overplotted in Figure 6. The best-fit value of the amplitude is  $K = 68.4 \pm 12.0 \text{ m s}^{-1}$ . This, coupled with the adopted stellar mass of  $1.213_{-0.063}^{+0.067} M_{\odot}$ , yields a planet mass of  $0.603_{-0.19}^{+0.13} M_{\text{J}}$ .

We also carried out fits in which the eccentricity was allowed to float. The best-fit model has an eccentricity = 0.24,  $K = 71.4 \text{ m s}^{-1}$ , yielding a planet mass of  $0.62 M_{\text{J}}$ . The RMS of the residuals is  $39 \text{ m s}^{-1}$  compared with  $40 \text{ m s}^{-1}$  for the circular orbit, rendering the eccentric orbit no better than the circular. Indeed a bootstrap Monte Carlo estimate of the parameter uncertainties gives a formal error in eccentricity of 0.16. We conclude that the eccentricity is consistent with zero, but could be as high as 0.4. This large uncertainty stems from the high  $v \sin i$  of the star and its relative faintness,  $V = 13.9 \text{ mag}$ .

A line bisector analysis showed no variation at a level of a few meters per second and no correlation with measured radial velocities. Thus, the velocity variation appears to represent actual acceleration of the center of mass of the star.

## 5. Properties of the Planet Kepler-8b

With the planet interpretation highly likely, the properties of the host star and the depth of transit directly yield a planet radius of  $1.419_{-0.058}^{+0.056} R_{\text{J}}$  and a mass of  $0.603_{-0.19}^{+0.13} M_{\text{J}}$ . The errors represent the 68%-probability domain of integrated uncertainty from all input measurements and models. The planet density is  $0.261 \pm 0.071 \text{ g cm}^{-3}$  apparently placing it among the low density exoplanets. Assuming a bond albedo of 0.1, its orbital radius of  $0.0483_{-0.0012}^{+0.0006} \text{ AU}$ , and the best-fit stellar luminosity from the Yale-Yonsei models gives an equilibrium temperature for the planet of  $1764 \pm 200 \text{ K}$ , assuming rapid and complete redistribution of thermal energy around the planet’s surface. This planet apparently is a member of the population of low density, bloated hot jupiters having thermal histories yet to be firmly understood. The planet properties are listed in Table 1.

## 6. Rossiter-McLaughlin Effect

The radial velocities obtained during the transit of 2009 October 29 (UT) were modeled using the techniques described by Cochran et al. (2008). The models adopted the system parameters in Table 1, and searched for the value of  $\lambda$  that best matched the observed velocities. In particular, we assumed the zero eccentricity orbit, as the *Kepler* photometric lightcurve gives no indication of non-zero eccentricity. We used a Claret (2004) four parameter limb-darkening law, although running similar models with both a linear and a quadratic limb-darkening law gave essentially the same results. We derive a value of  $\lambda = -26.9 \pm 4.6^{\circ}$  for the angle between the projected stellar rotation

axis and the projected planetary orbital axis. The model fit to the data gives a reduced chi-squared  $\chi_0^2 = 0.66$  for the velocities obtained during the transit, indicating that the uncertainties in these velocities are probably slightly overestimated.

The radial velocities measured during the transit and the Rossiter-McLaughlin effect model fit are shown in Figure 7. The observed asymmetric Rossiter-McLaughlin effect, with a positive deviation of larger amplitude and longer duration than the negative amplitude is a result of the combination of the large impact parameter and the non-zero value of  $\lambda$ . A central transit would give a symmetric Rossiter-McLaughlin deviation, with the amplitude of the effect then depending on  $\lambda$ . However, for an off-center transit, the overall shape depends critically on both the impact parameter and on  $\lambda$  (cf. Figure 2 of Gaudi & Winn (2007)).

This Rossiter-McLaughlin analysis provides independent verification of the major results of the transit lightcurve analysis. The lightcurve analysis alone suggested a transit chord that is significantly off-center, with impact parameter,  $b = 0.724 \pm 0.020$  and inclination,  $i = 84.07 \pm 0.33$ . This large impact parameter coupled with the non-zero value of  $\lambda$  results in the planet transit blocking mostly the approaching (blue-shifted) half of the rotating star, as indicated in 8. The planet crosses to the receding (red-shifted) portion of the stellar disk just before the end of the transit. This causes the observed asymmetry in the Rossiter McLaughlin velocity perturbation during the transit. The observed amplitude of the R-M effect is in excellent agreement with the photometrically determined stellar radius and impact parameter, and with the spectroscopically determined  $v \sin i$ . The duration of the photometric transit agrees with the duration of the observed R-M velocity perturbation. This consistency between the properties of the system as derived from the transit photometry and from the R-M velocity perturbation gives a confirmation that both phenomena were caused by an orbiting, planet-sized companion to the star. There is no other explanation of the observed R-M variations that is also consistent with both the photometric and the radial velocity observations.

This observation of the Rossiter-McLaughlin effect in Kepler-8 is important because it confirms that the observed lightcurve and radial velocity variations in Kepler-8 were indeed caused by an orbiting planetary companion. The amount of scatter in the radial velocity data giving the solution shown in Figure 6 is uncomfortably large, even given the lack of line bisector variations in these spectra. However, the R-M data absolutely confirm the existence of the planet. There is no other explanation of the observed R-M variations that is also consistent with both the photometric, astrometric, imaging, and the radial velocity observations.

## 7. DISCUSSION

We have carried out a wide array of observations of Kepler-8 that pinpoint the existence and properties of the exoplanet. The *Kepler* photometric measurements, with  $\sim 0.1$  mmag errors in 30 min intervals, are tightly fit by a model of a transiting exoplanet (Figure 1). This good fit to the

inflections of the photometric data provide immediate support for the planet interpretation, with few plausible alternative interpretations except for a background, diluted eclipsing binary system having just the right brightness and radius ratio to mimic a planet. We note that, unlike ground-based transit work that has lower photometric precision, the *Kepler* photometry is so precise that blends of eclipsing binaries are more readily identified from the photometry alone.

Nonetheless, to test the unlikely possibility of a blend, we carried out a battery of astrometric tests to hunt for an eclipsing binary. The resulting steadiness of the position of the primary star, Kepler-8, during and out of transit, argues against any eclipsing binary in the photometric aperture. We further carried out both adaptive optics imaging and speckle interferometric measurements to hunt for faint eclipsing binaries located within an arcsec of the Kepler-8. None was found, further diminishing the chance of such a masquerade. We followed with high resolution spectroscopy at both low and high signal-to-noise ratio, finding no evidence of double lines nor rapid rotation. Further support for the planet interpretation came from the precise radial velocities that varied in phase with, and had the same period as, the photometric light curve, further supporting the planet model and constraining the planet mass.

Finally, the Rossiter-McLaughlin effect confirmed independently the planet interpretation and provided further geometrical information about the orbit, notably  $\lambda = -26.9 \pm 4.6^\circ$ . A sketch of the star and planet's orbit are shown in (Figure 8). Remaining unknown is the inclination of the star's rotation axis, as indicated in 8. But continued photometry during the *Kepler* mission lifetime may reveal a photometric periodicity caused by the rotation of spots around the star. The resulting rotation period, coupled with the measured rotational  $v \sin i = 10.5 \pm 0.7$  of the star, will allow the star's inclination to be measured, putting the R-M geometry on firmer ground.

The suite of ground-based observations obtained for Kepler-8 described above over-constrained a set of parameters that were obligated to mutually agree, including such subtle issues as the limb-darkening, the stellar rotation rate, and stellar radius, mass, and density. Thus, the R-M effect can, in general, be used to confirm the existence of a planetary companion in the case where standard follow-up observing procedures may provide somewhat ambiguous or equivocal results. Examples would be *Kepler* stars that are sufficiently saturated that measurement of photocenter shifts during transits is problematic, or stars like Kepler-8 with large  $v \sin i$  that make orbit determination via precise RV measurement difficult.

Observations of the Rossiter-McLaughlin effect in dozens of transiting planets, discovered from the ground and from *Kepler*, offer an excellent opportunity to determine the distribution of orbital geometries of the short-period planetary systems in general. These planetary systems will continue to be studied in an extraordinarily uniform and consistent manner with the same set of tools. The sample selection effects are extremely well understood and documented. The *Kepler* lightcurves are of unprecedented precision, allow sensitive searches for additional planets in the system via transit timing variations, and significantly tighter limits to be placed in the future on the orbital eccentricity. Coupling these data with R-M measurements of the orbital alignment in these systems

will allow us to correlate the observed properties with the degree of orbital alignment, and thus to search for the physical mechanisms causing observed misalignments. We will also have the information to be able to begin to back-out the physical angle between the spin and orbital angular momentum vectors, not just the projection of these angles on the plane of the sky.

Funding for this Discovery mission is provided by NASA’s Science Mission Directorate. Many people have contributed to the success of the *Kepler Mission*, and it is impossible to acknowledge them all. Valuable advice and assistance were provided by Willie Torres, Riley Duren, M. Crane, and D. Ciardi. Special Technical help was provided by Carly Chubak, G. Mandushev, and Josh Winn. We thank E. Bachtel and his team at Ball Aerospace for their work on the *Kepler* photometer and R. Thompson for key contributions to engineering; and C. Botosh, and J. Fanson, for able management. GWM thanks acknowledges support from NASA Cooperative Agreement NNX06AH52G.

*Facilities:* Kepler.

## REFERENCES

- Adams, F. C. & Laughlin, G. 2003, *Icarus*, 163, 290
- Amaury et al. arxiv0907.2956
- Anderson, D. R., et al. ApJ submitted, arXiv0908.1553
- Bakos, G. Á., et al. 2007, ApJ, 670, 826
- Barbieri, M., et al. 2009, A&A, 503, 601
- Batalha, N. M., et al. 2010 ApJL Submitted
- Borucki, W. et al. 2010, Science Submitted
- Borucki, et al. 2010, ApJL Submitted
- Bouchy, F., Queloz, D., Deleuil, M., Loeillet, B., Hatzes, A. P., Aigrain, S., Alonso, R., Auvergne, M., Baglin, A., Barge, P., Benz, W., Bordé, P., Deeg, H. J., De la Reza, R., Dvorak, R., Erikson, A., Fridlund, M., Gondoin, P., Guillot, T., Hébrard, G., Jorda, L., Lammer, H., Léger, A., Llebaria, A., Magain, P., Mayor, M., Moutou, C., Ollivier, M., Pätzold, M., Pepe, F., Pont, F., Rauer, H., Rouan, D., Schneider, J., Triaud, A. H. M. J., Udry, S., & Wuchterl, G. 2008, ArXiv e-prints, 0803.3209
- Brown, T. M., et al. 2010, ApJL Submitted
- Charbonneau, D., Winn, J. N., Everett, M. E., Latham, D. W., Holman, M. J., Esquerdo, G. A., & O’Donovan, F. T. 2007, ApJ, 658, 1322

- Chatterjee, A., Sarkar, A., Barat, P., Mukherjee, P., & Gayathri, N. 2008, ArXiv e-prints, 0804.1670
- Cochran, W. D., Redfield, S., Endl, M., & Cochran, A. L. 2008, ApJ, 683, L59
- Claret, A. 2004, A&A, 428, 1001
- Demarque, P., Woo, J.-H., Kim, Y.-C., & Yi, S. K. 2004, ApJS, 155, 667
- Dunham, E. W., et al 2010 ApJL Submitted
- Fabrycky, D. & Tremaine, S. 2007, ApJ, 669, 1298
- Fabrycky, D. C., & Winn, J. N. 2009, ApJ, 696, 1230
- Gaudi, B. S. & Winn, J. N. 2007, ApJ, 655, 550
- Gautier, T. N., et al. 2010, ApJL, in press
- Gillon, M. 2009, archiv0906.4904
- Giménez, A. 2006, ApJ, 650, 408
- Hayward, T. L., Brandl, B., Pirger, B., Blacken, C., Gull, G. E., Schoenwald, J., & Houck, J. R. 2001, PASP, 113, 105
- Hébrard, G., et al. 2009, IAU Symposium, 253, 508
- Holman, M., Touma, J., & Tremaine, S. 1997, Nature, 386, 254
- Jenkins et al. 2010, ApJL, in press
- Johnson, J. A., et al. 2008, ApJ, 686, 649
- Johnson, J. A., Winn, J. N., Albrecht, S., Howard, A. W., Marcy, G. W., & Gazak, J. Z. 2009, PASP, 121, 1104
- Joshi, Y. C., et al. 2009, MNRAS, 392, 1532
- Koch et al. 2010, ApJL, in press
- Koch, et al. 2010, ApJL, in press
- Kobayashi, Y., Yoshii, Y., Peterson, B. A., Minezaki, T., Enya, K., Suganuma, M., & Yamamuro, T. 1998, 3354, 769
- Lin, D. N. C., Bodenheimer, P., & Richardson, D. C. 1996, Nature, 380, 606

- Loeillet, B., Shporer, A., Bouchy, F., Pont, F., Mazeh, T., Beuzit, J. L., Boisse, I., Bonfils, X., da Silva, R., Delfosse, X., Desort, M., Ecuivillon, A., Forveille, T., Galland, F., Gallenne, A., Hébrard, G., Lagrange, A.-M., Lovis, C., Mayor, M., Moutou, C., Pepe, F., Perrier, C., Queloz, D., Ségransan, D., Sivan, J. P., Santos, N. C., Tsodikovich, Y., Udry, S., & Vidal-Madjar, A. 2008, *A&A*, 481, 529
- Mandel, K. & Agol, E. 2002, *ApJ*, 580, L171
- Marcy, G. W., et al. 2008, *Physica Scripta Volume T*, 130, 014001
- Minezaki, T., Yoshii, Y., Kobayashi, Y., Enya, K., Sukanuma, M., Tomita, H., Aoki, T., & Peterson, B. A. 2004, *ApJ*, 600, L35
- Moorhead, A. V. & Adams, F. C. 2008, *Icarus*, 193, 475
- Moutou, C., et al. 2009, *A&A*, 498, L5
- Nagasawa, M., Ida, S., & Bessho, T. 2008, *ArXiv e-prints*, 0801.1368
- Narita, N., Enya, K., Sato, B., Ohta, Y., Winn, J. N., Suto, Y., Taruya, A., Turner, E. L., Aoki, W., Yoshii, M., Yamada, T., & Tamura, Y. 2007a, *PASJ*, 59, 763
- Narita, N., Sato, B., Ohshima, O., & Winn, J. N. 2007, *ArXiv e-prints*, 0712.2569
- Narita, N., Sato, B., Hirano, T., & Tamura, M. 2009, *PASJ*, 61, L35
- Narita, N., et al. 2009, *PASJ*, 61, 991
- Noguchi, K., Aoki, W., Kawanomoto, S., Ando, H., Honda, S., Izumiura, H., Kambe, E., Okita, K., Sadakane, K., Sato, B., Tajitsu, A., Takada-Hidai, T., Tanaka, W., Watanabe, E., & Yoshida, M. 2002, *PASJ*, 54, 855
- Ohta, Y., Taruya, A., & Suto, Y. 2005, *ApJ*, 622, 1118
- Pal, A. et al. 2010, *MNRAS*, in press.
- Papaloizou, J. C. B. & Terquem, C. 2001, *MNRAS*, 325, 221
- Pont, F., et al. 2009, *arXiv0908.3032*
- Pont, F., et al. 2009, *A&A*, 502, 695
- Pont, F., et al. 2009, *MNRAS*, L360
- Prša, A., & Zwitter, T. 2006, *Ap&SS*, 304, 347.
- Queloz, D., Eggenberger, A., Mayor, M., Perrier, C., Beuzit, J. L., Naef, D., Sivan, J. P., & Udry, S. 2000, *A&A*, 359, L13

- Rasio, F. A. & Ford, E. B. 1996, *Science*, 274, 954
- Pál, A., et al. 2008, *ApJ*, 680, 1450
- Rowe, J. F., et al. 2010, *ApJL* Submitted
- Simpson, E.K., Pollacco, D. and Hebrard, G. and Gibson, N.P. and Barros, S.C.C. and Bouchy, F. and Collier Cameron, A. and Boisse, I. and Watson, C.A., and Keenan, F., [arXiv.org/0912.3643](https://arxiv.org/abs/0912.3643)
- Skrutskie, M. J., et al. 2006, *AJ*, 131, 1163
- Southworth, J. 2008, *ArXiv e-prints*, 0802.3764
- Sozzetti, A., Torres, G., Charbonneau, D., Latham, D. W., Holman, M. J., Winn, J. N., Laird, J. B., & O'Donovan, F. T. 2007, *ApJ*, 664, 1190
- Torres, G., Winn, J. N., & Holman, M. J. 2008, *ApJ*, 677, 1324
- Valenti, J. A., & Piskunov, N. 1996, *A&AS*, 118, 595
- Valenti, J. A., & Fischer, D.A. 2005, *ApJS*, 159, 141
- Vogt, S. S., Allen, S. L., Bigelow, B. C., Bresee, L., Brown, B., Cantrall, T., Conrad, A., Couture, M., Delaney, C., Epps, H. W., Hilyard, D., Hilyard, D. F., Horn, E., Jern, N., Kanto, D., Keane, M. J., Kibrick, R. I., Lewis, J. W., Osborne, J., Pardeilhan, G. H., Pfister, T., Ricketts, T., Robinson, L. B., Stover, R. J., Tucker, D., Ward, J., & Wei, M. Z. 1994, in *Proc. SPIE Instrumentation in Astronomy VIII*, David L. Crawford; Eric R. Craine; Eds., Volume 2198, p. 362, ed. D. L. Crawford & E. R. Craine, 362+
- Ward, W. R. & Hahn, J. M. 1994, *Icarus*, 110, 95
- Winn, J. N., Noyes, R. W., Holman, M. J., Charbonneau, D., Ohta, Y., Taruya, A., Suto, Y., Narita, N., Turner, E. L., Johnson, J. A., Marcy, G. W., Butler, R. P., & Vogt, S. S. 2005, *ApJ*, 631, 1215
- Winn, J. N., Johnson, J. A., Marcy, G. W., Butler, R. P., Vogt, S. S., Henry, G. W., Roussanova, A., Holman, M. J., Enya, K., Narita, N., Suto, Y., & Turner, E. L. 2006, *ApJ*, 653, L69
- Winn, J. N., Holman, M. J., & Fuentes, C. I. 2007b, *AJ*, 133, 11
- Winn, J. N., Johnson, J. A., Peek, K. M. G., Marcy, G. W., Bakos, G. Á., Enya, K., Narita, N., Suto, Y., Turner, E. L., & Vogt, S. S. 2007c, *ApJ*, 665, L167
- Winn, J., et al. 2007, *ApJ*, 657, 1098
- Winn, J. N., Johnson, J. A., Narita, N., Suto, Y., Turner, E. L., Fischer, D. A., Butler, R. P., Vogt, S. S., O'Donovan, F. T., & Gaudi, B. S. 2008, *ArXiv e-prints*, 804.2259

Winn, J. N., et al. 2009, *ApJ*, 700, 302

Winn, J. N., et al. 2009, *ApJ*, 703, 2091

Winn, J. N., Johnson, J. A., Albrecht, S., Howard, A. W., Marcy, G. W., Crossfield, I. J., & Holman, M. J. 2009, *ApJ*, 703, L99

Wolf, A. S., Laughlin, G., Henry, G. W., Fischer, D. A., Marcy, G., Butler, P., & Vogt, S. 2007, *ApJ*, 667, 549

Wright, J. T., Upadhyay, S., Marcy, G. W., Fischer, D. A., Ford, E. B., & Johnson, J. A. 2009, *ApJ*, 693, 1084

Wu, Y., Murray, N. W., & Ramsahai, J. M. 2007, *ApJ*, 670, 820

Yi, S. K., Demarque, P., Kim, Y.-C., Lee, Y.-W., Ree, C. H., Lejeune, T., & Barnes, S. 2001, *ApJS*, 136, 417

Table 1. System Parameters for Kepler-8

Parameter	Value	Notes
<i>Transit and orbital parameters</i>		
Orbital period $P$ (d)	$3.52254^{+0.00003}_{-0.00005}$	A
Midtransit time $E$ (HJD)	$2454954.1182^{+0.0003}_{-0.0004}$	A
Scaled semimajor axis $a/R_*$	$6.97^{+0.20}_{-0.24}$	A
Scaled planet radius $R_P/R_*$	$0.09809^{+0.00040}_{-0.00046}$	A
Impact parameter $b \equiv a \cos i/R_*$	$0.724 \pm 0.020$	A
Orbital inclination $i$ (deg)	$84.07 \pm 0.33$	A
Orbital semi-amplitude $K$ ( $\text{m s}^{-1}$ )	$68.4 \pm 12.0$	A,B
Orbital eccentricity $e$	0 (adopted)	A,B
<i>Observed stellar parameters</i>		
Effective temperature $T_{\text{eff}}$ (K)	$6213 \pm 150$	C
Spectroscopic gravity $\log g$ (cgs)	$4.28 \pm 0.10$	C
Metallicity [Fe/H]	$-0.055 \pm 0.03$	C
Projected rotation Velocity $v \sin i$ ( $\text{km s}^{-1}$ )	$10.5 \pm 0.7$	C
Absolute (Helio) radial velocity ( $\text{km s}^{-1}$ )	$-52.72 \pm 0.10$	B
<i>Derived stellar parameters</i>		
Mass $M_*$ ( $M_\odot$ )	$1.213^{+0.067}_{-0.063}$	C,D
Radius $R_*$ ( $R_\odot$ )	$1.486^{+0.053}_{-0.062}$	C,D
Surface gravity $\log g_*$ (cgs)	$4.174 \pm 0.026$	C,D
Luminosity $L_*$ ( $L_\odot$ )	$4.03^{+0.52}_{-0.54}$	C,D
Absolute V magnitude $M_V$ (mag)	$3.28 \pm 0.15$	D
Age (Gyr)	$3.84 \pm 1.5$	C,D
Distance (pc)	$1330 \pm 180$	D
<i>Planetary parameters</i>		
Mass $M_P$ ( $M_J$ )	$0.603^{+0.13}_{-0.19}$	A,B,C,D
Radius $R_P$ ( $R_J$ )	$1.419^{+0.056}_{-0.058}$	A,BC,D
Density $\rho_P$ ( $\text{g cm}^{-3}$ )	$0.261 \pm 0.071$	A,B,C,D
Surface gravity $\log g_P$ (cgs)	$2.871 \pm 0.119$	A,B,C,D
Orbital semimajor axis $a$ (AU)	$0.0483^{+0.0006}_{-0.0012}$	E
Equilibrium temperature $T_{\text{eq}}$ (K)	$1764 \pm 200$	F

Note. —

A: Based on the photometry.

B: Based on the radial velocities.

C: Based on an SME analysis of the Keck-HIRES spectra,

D: Based on the Yale-Yonsei stellar evolution tracks.

E: Based on Newton's version of Kepler's Third Law and total mass.

F: Assumes Bond albedo = 0.1 and complete redistribution.

Table 2. Relative Doppler Velocity Measurements of Kepler-8

HJD (-2450000)	RV (m s <sup>-1</sup> )	$\sigma_{\text{RV}}$ (m s <sup>-1</sup> )
4984.040	-22.15	34.5
4985.043	52.45	34.5
4986.065	-42.39	34.0
4987.060	-74.37	33.6
4988.027	63.04	33.7
4988.973	98.87	33.8
4995.103	46.58	34.2
5014.891	-64.61	33.7
5015.975	-29.97	33.4
5017.020	-28.28	33.3
5075.788	41.65	33.9
5109.850	-122.00	32.8
5110.790	-67.42	31.9
5133.839	49.58	32.8
5133.718	58.11	32.6
5133.732	51.13	32.5
5133.747	71.85	32.7
5133.761	34.51	32.8
5133.776	24.38	32.6
5133.790	-9.49	33.2
5133.805	-31.04	33.2
5133.821	-14.32	32.6
5134.740	-23.48	31.9
5135.790	48.50	32.6

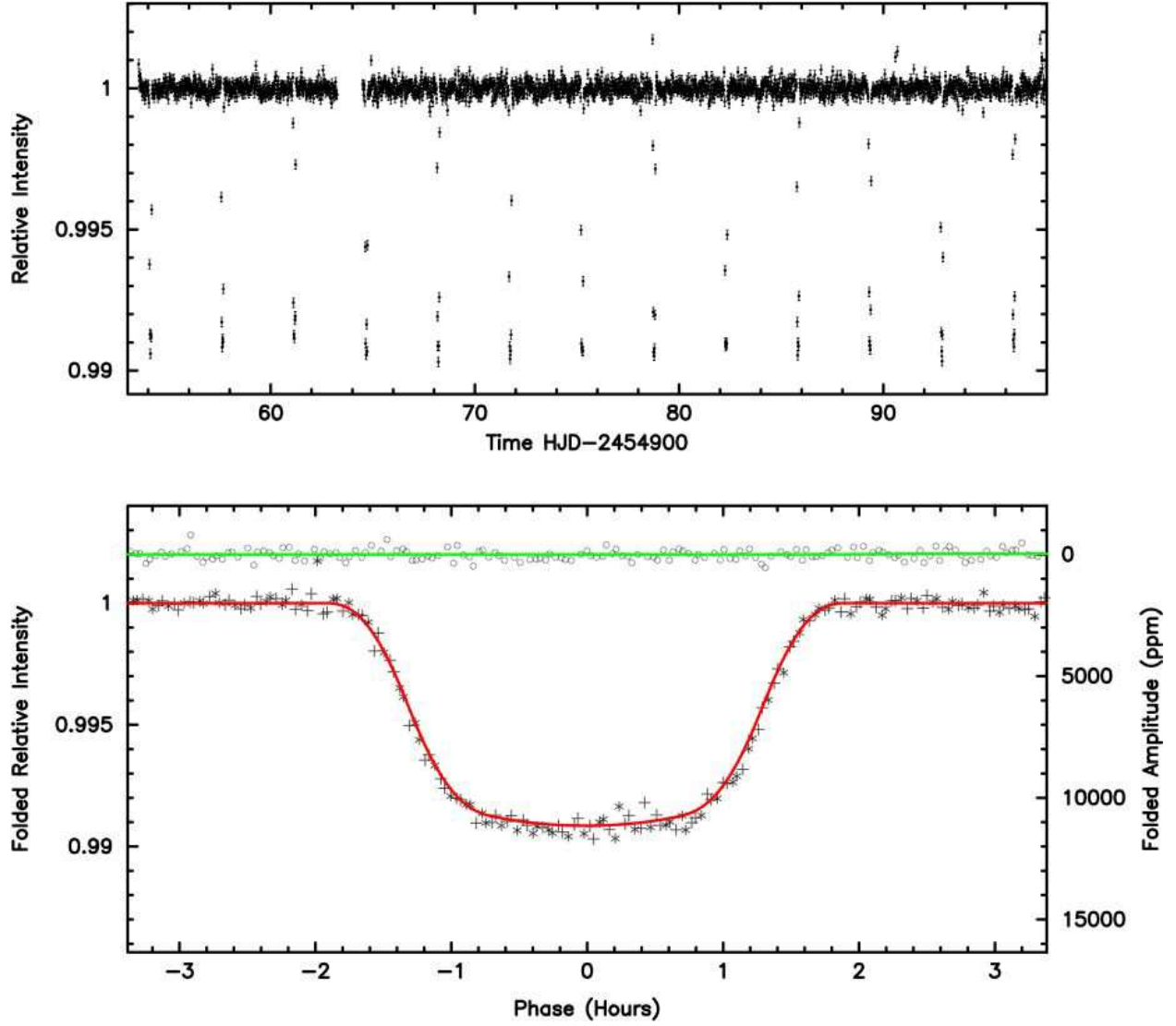


Fig. 1.— The detrended light curve for Kepler-8. The time series for the entire *Kepler* photometric data set is plotted in the upper panel. The lower panel shows the photometry folded by the period  $P = 3.52254$  days, and the model fit to the primary transit is plotted as a solid line. Data for even and for odd transits are denoted by '+'s and '\*'s, respectively. The even and odd transits do not exhibit significant variations in transit depth indicative of the primary and secondary eclipses of an eclipsing binary. The photometry at the predicted time of occultation of the planet is shown just above the phased transit curve, showing no significant dimming at the level of 0.1 mmag. The lack of any dimming at the predicted time of occultation, along with the absence of both astrometric motion in and out of transit and the absence of detected stellar companions, leaves the planetary interpretation as the only plausible model, confirmed by the Rossiter-McLaughlin detection.

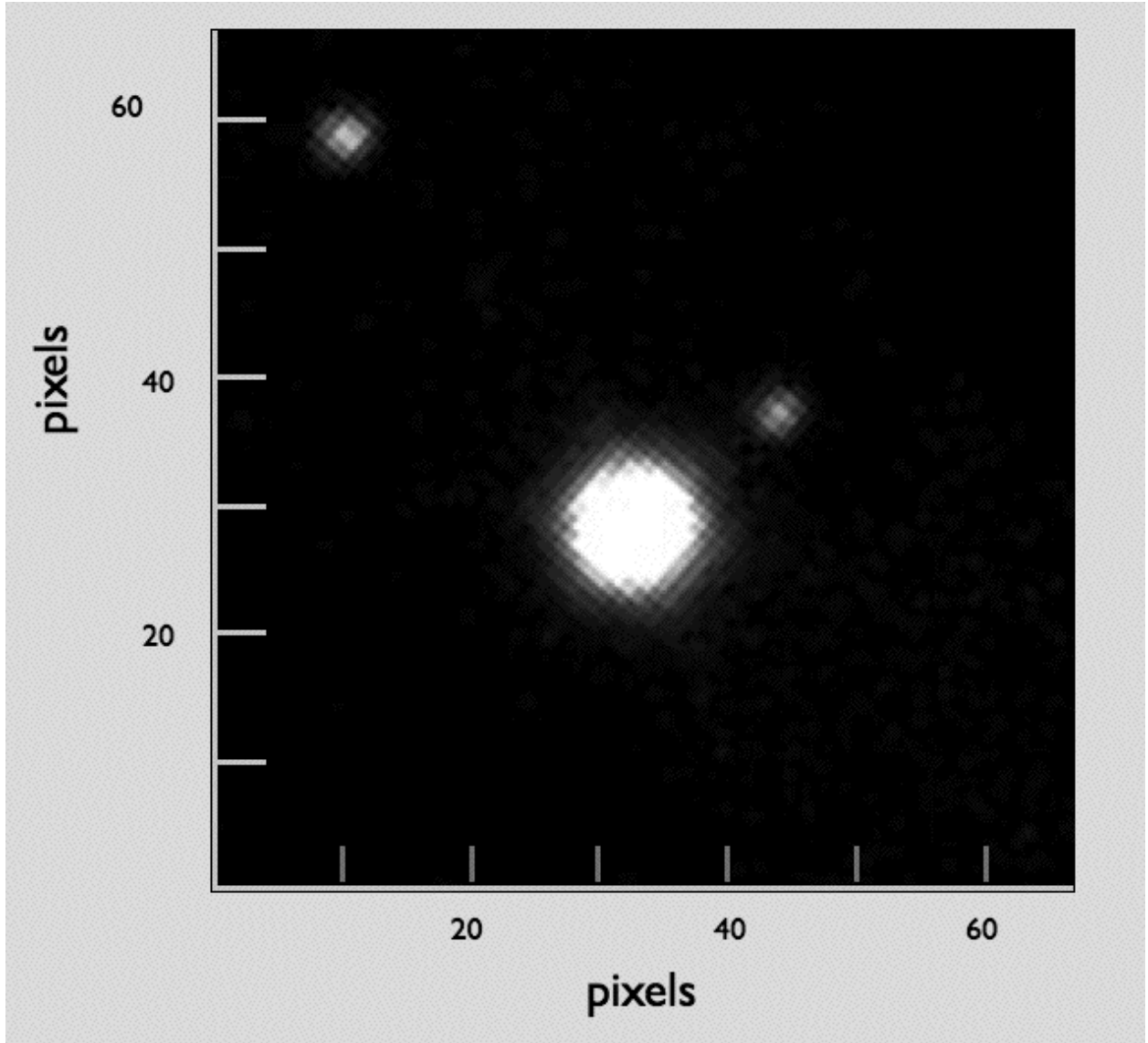


Fig. 2.— The image of the field near Kepler-8 obtained from the Keck 1 telescope guider camera with a bg38 filter, making the bandpass approximately V and R combined, similar to that of the *Kepler* photometer. North is up, and east to the left, and the plate scale is  $0.397''$  per pixel. The main star, Kepler-8 is the brightest source at the center of the image. A faint star is located  $3.8''$  to the northwest of Kepler-8, having a flux 0.75% that of Kepler-8 and residing within the *Kepler* photometric aperture. With a flux less than 1% that of Kepler-8, the companion cannot be responsible for the periodic 1% dimming, even if it were a background eclipsing binary. But this neighboring star is sufficiently bright to account for the astrometric displacement of the Kepler-8 that occurs during transit of its planet, explaining the shift of the photocenter of the two stars by  $0.0001$  *Kepler* pixels.

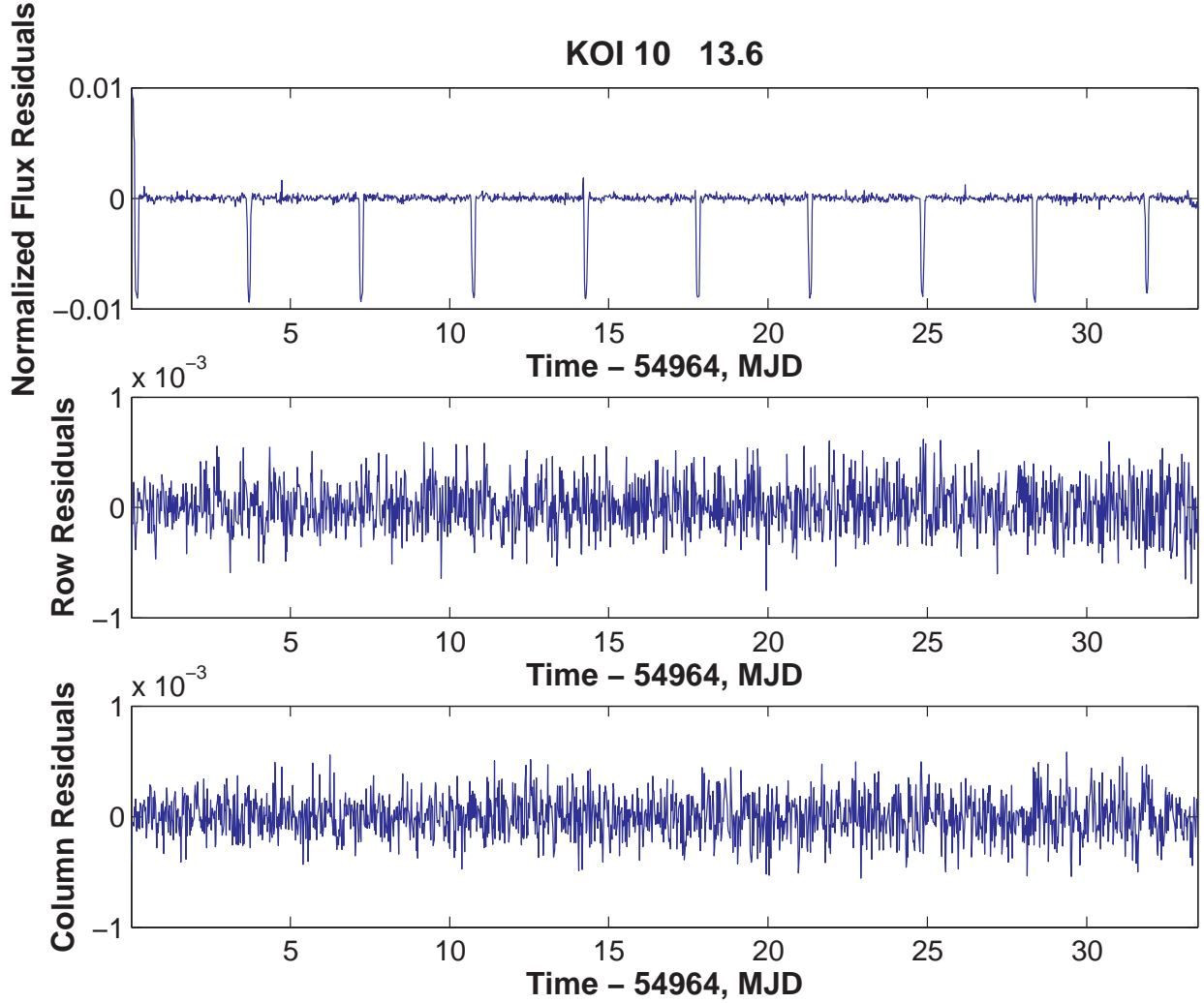


Fig. 3.— Flux(upper) and astrometric centroid (middle, lower) timeseries of Kepler-8b from *Kepler* quarter-1 data. A high-pass filter has been applied to each time series to remove non-transit signatures on timescales longer than 2 days. There is no obvious displacement of the centroid of light in either the row or column residuals. This lack of motion indicates that any background eclipsing binary would need to be located within  $\sim 0.001/.01 = 0.1$  pixels corresponding to  $0.4''$  of the target star in order to explain the photometric transit signals but avoid showing motion.

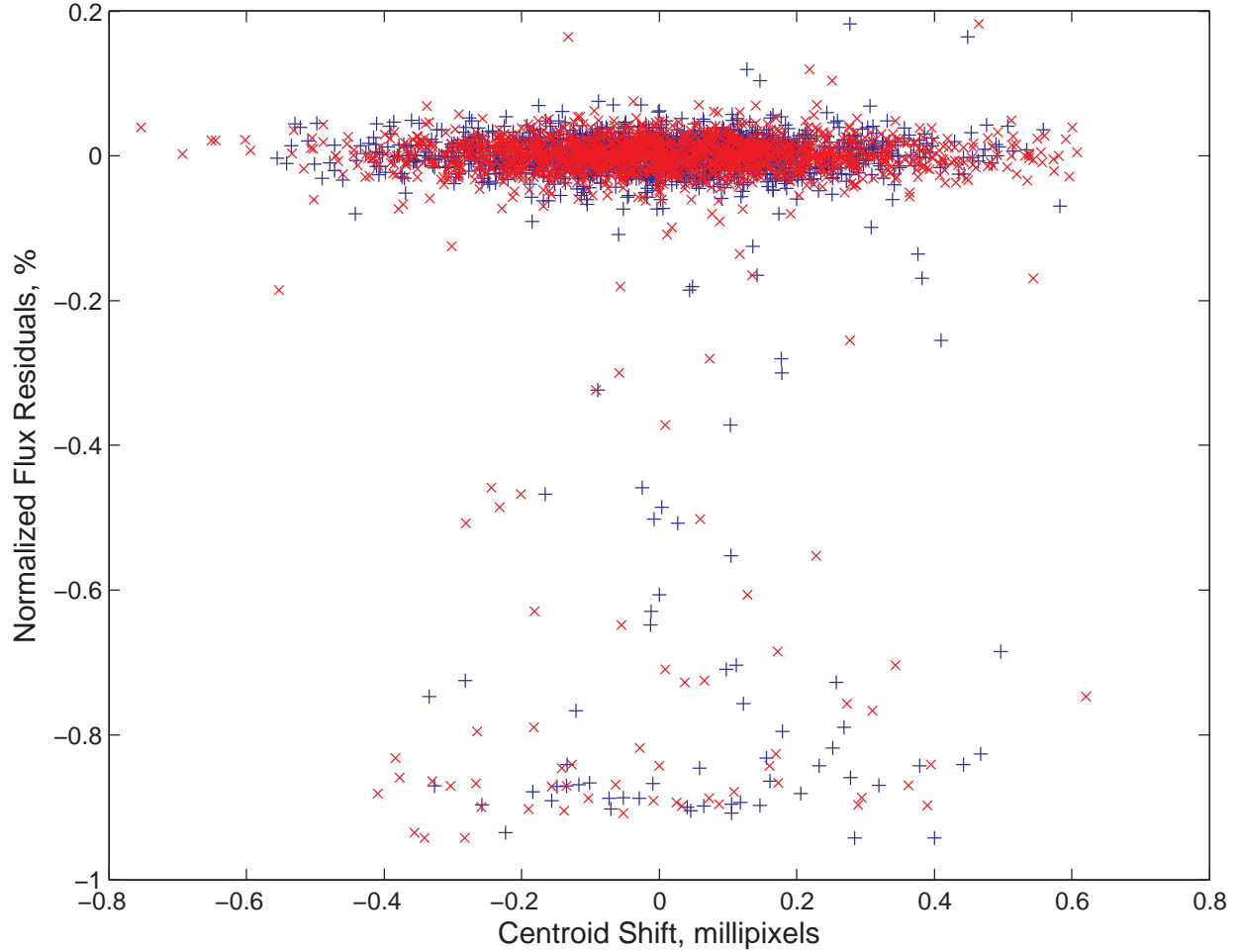


Fig. 4.— Flux versus residual astrometric centroids in row (x) and column (+) for Kepler-8. The measurements are the same as those presented in Figure 3. This “rainplot” shows no evidence that the centroids are systematically shifting during each transit event, which would be indicative of a blend with a background star. If this were the case, identification of the actual star responsible for the transit features in the light curve would require inspection of a high resolution image or catalog to unravel the mystery. Since the in-transit points “rain” straight down, rather than slanting along a diagonal, any blend scenario would require a very small separation on the sky between the two sources.

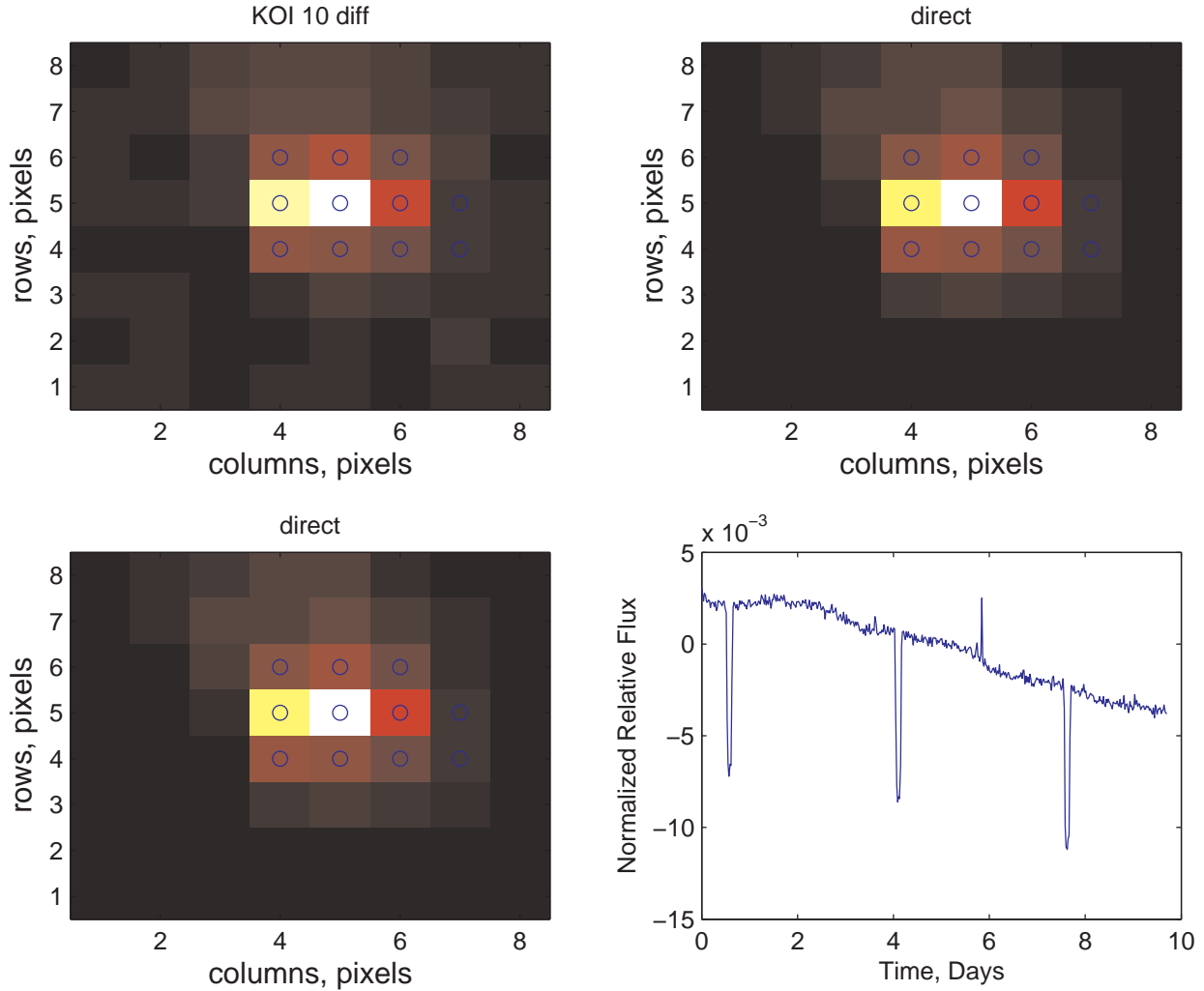


Fig. 5.— The results of a ”poor man’s” difference image analysis are presented in this figure: (A) (upper left) is the result of subtracting the average of the in-transit images from the average of a similar number of just out-of-transit images for one of Kepler-8b’s transits. The pixels summed to form the photometric brightness measurements are indicated by the blue circles. For comparison, the average of the out-of-transit images are displayed in (B – upper right) and (C – lower left). The raw flux light curve from Q0 is displayed panel (D – lower right). The difference image, Panel (A) is remarkably similar to the direct images. Had the transits been due to a background eclipsing binary that were 0.5 or more pixels offset from the target star, then the difference image would display a noticeable shift in the location of the pixel containing the peak energy. Instead, both difference and direct images supporting a coincident localization of the source of the transits to the target star, Kepler-8.

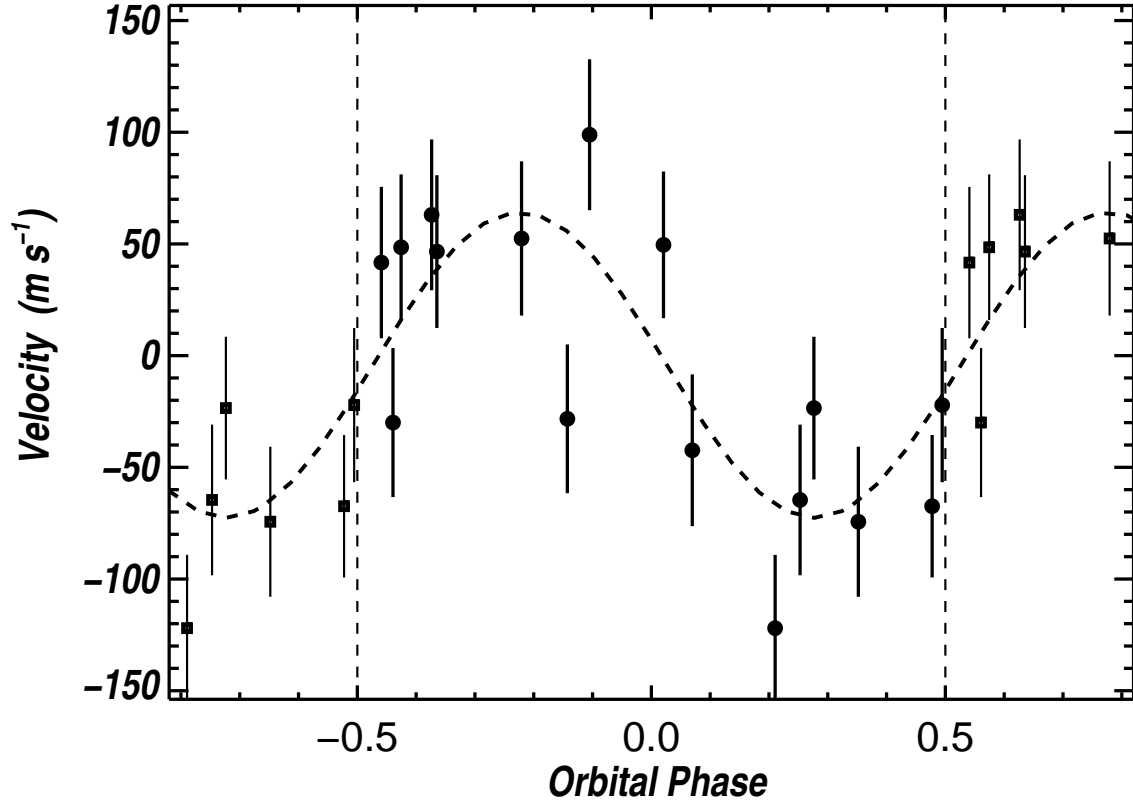


Fig. 6.— The orbital solution for Kepler-8. The observed radial velocities obtained with HIRES on the Keck 1 Telescope are plotted together with the best-fit velocity curve for a circular orbit with the period and time of transit fixed by the photometric ephemeris. Uncertainties are large due to the faintness of the star ( $V=13.9$  mag), the high rotational Doppler broadening ( $v \sin i= 10.5 \pm 0.7$ ), and contamination from background moonlight in most spectra. The measured velocities vary high and low as predicted by the orbit from the photometric transit curve, supporting the planet model.

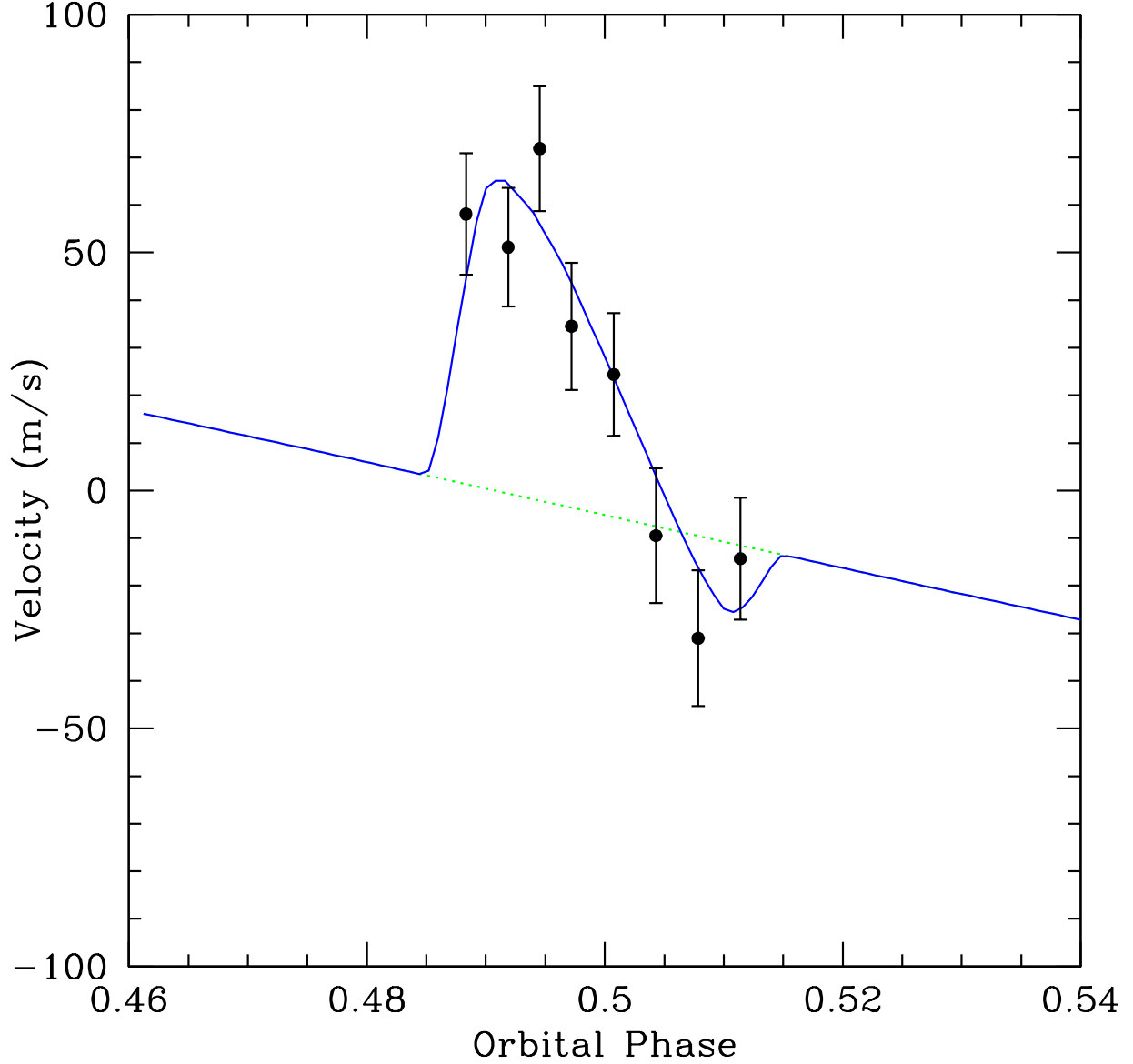


Fig. 7.— The Rossiter-McLaughlin effect for Kepler-8. The observed radial velocities obtained with HIRES on the Keck 1 Telescope are plotted together with the predicted velocities from the best-fit model of the Rossiter-McLaughlin effect. The high velocities near ingress and low velocities near egress imply a prograde orbit. The asymmetry in the model curve indicates a projected tilt of the orbit relative to the star’s equator, as well as a transit with a large impact parameter on the star.

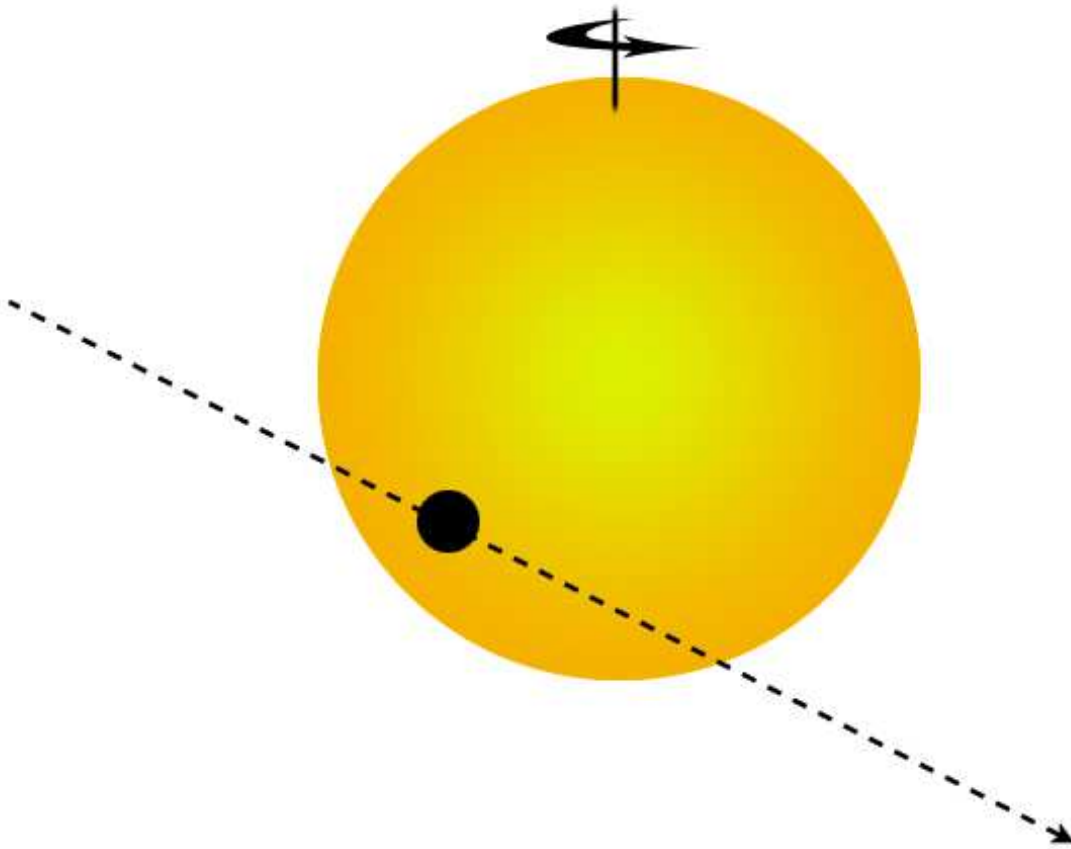


Fig. 8.— A sketch of the transit geometry for Kepler-8. The *Kepler* photometry and R-M measurements set the impact parameter,  $b = 0.724 \pm 0.020$ , and the angle projected on the sky between the star's spin axis and the normal to the orbital plane,  $\lambda = -27^\circ$ , indicating a prograde orbit with a moderate inclination.